Dalton Transactions

ROYAL SOCIETY OF CHEMISTRY

PAPER

View Article Online
View Journal | View Issue

Cite this: *Dalton Trans.*, 2023, **52**, 11325

Variation in pnictogen–oxygen bonding unlocks greatly enhanced Brønsted basicity for the monomeric stibine oxide†

John S. Wenger, Addis Getahun and Timothy C. Johnstone *

Phosphine oxides and arsine oxides feature highly polarized pnictoryl groups (Pn^{+}–O^{-}/Pn = O; Pn = P, As) and react as Brønsted bases through O-centered lone pairs. We recently reported the first example of a monomeric stibine oxide, $Dipp_3SbO$ (Dipp = diisopropylphenyl), allowing periodic trends in pnictoryl bonding to be extended to antimony for the first time. Computational studies suggest that, as the pnictogen atom becomes heavier, delocalization of electron density from the O-centered lone pairs to the Pn–C σ* orbitals is attenuated, destabilizing the lone pairs and increasing the donor capacity of the pnictine oxide. Herein, we assess the Brønsted basicity of a series of monomeric pnictine oxides ($Dipp_3PnO$; Pn = P, As, and Sb). Stoichiometric reactivity between $Dipp_3PnO$ and a series of acids demonstrates the greatly enhanced ability of $Dipp_3SbO$ to accept protons relative to the lighter congeners, consistent with theoretical isodesmic reaction enthalpies and proton affinities. ^{1}H NMR spectrometric titrations allow for the $pK_{aH,MeCN}$ determination of $Dipp_3AsO$ and $Dipp_3SbO$, revealing a 10^{6}-fold increase in Brønsted basicity from $Dipp_3AsO$ to $Dipp_3SbO$. The increased basicity can be exploited in catalysis; $Dipp_3SbO$ exhibits dramatically increased catalytic efficiency in the Brønsted base-catalyzed transesterification between *p*-nitrophenyl acetate and 2,2,2-trifluoroethanol. Our results unambiguously confirm the drastic increase in Brønsted basicity from $Dipp_3PO$ < $Dipp_3AsO$ < $Dipp_3SbO$, a direct consequence of the variation in the electronic structure of the pnictoryl bond as the pnictogen atom increases in atomic number.

Received 5th July 2023,
Accepted 27th July 2023

DOI: 10.1039/d3dt02113k

rsc.li/dalton

Introduction

Evaluation of periodic trends provides chemists with fundamental insights into chemical behavior, guides research, and informs chemical education strategies.[1] The synthesis and isolation of novel chemical motifs provide an opportunity to extend these trends and expand the frontier of modern chemistry. Main-group chemistry is in a state of renaissance following a number of seminal discoveries that highlight the ability of compounds bearing p-block elements to exhibit much of the rich reactivity that was once thought to be reserved for transition-metal complexes.[2–5] Organopnictogen compounds, in particular, have been identified as promising candidates for main-group redox catalysis.[6] Recent years have witnessed landmark achievements in the development of phosphorus(III/V) catalytic processes, largely through rational ligand design. Exemplary catalytic platforms include ring-strained phosphines that catalyze Wittig reactions and a C_s-symmetric σ^3-phosphorous triamide that catalyzes C–X substitution through an oxidative addition/reductive elimination pathway.[7,8] Advancements in phosphorus redox catalysis have been complemented by the more recent development of bismuth-based redox-cycling catalytic platforms.[9–18]

Phosphine oxides (oxo-λ^5-phosphanes) are a staple class of pnictogen compounds and feature in a wide array of different fields of chemistry. For over a century, they have served as stable by-products that are generated stoichiometrically to drive forward chemical reactions, including those discovered by Wittig,[19] Mitsunobu,[20] Appel,[21] and Staudinger.[22] The O-centered lone-pairs of phosphine oxides allow these species to act as versatile hard Lewis bases. Synthetic access to structurally diverse phosphine oxides has allowed for their extensive exploration and development as efficient organocatalysts for a range of processes, including enantioselective transformations.[23] The coordination chemistry of phosphine oxides has been utilized in catalysis,[24,25] supramolecular synthesis,[26] and uranium capture.[27] The stability and Lewis basicity of triethylphosphine oxide is commonly exploited to evaluate the strength of Lewis acids in the Gutmann–Beckett method, where the chemical shift of the ^{31}P nucleus serves as a con-

Department of Chemistry and Biochemistry, University of California Santa Cruz, Santa Cruz, California 95064, USA. E-mail: johnstone@ucsc.edu

†Electronic supplementary information (ESI) available. CCDC 2250578–2250587. For ESI and crystallographic data in CIF or other electronic format see DOI: https://doi.org/10.1039/d3dt02113k

venient spectroscopic handle.[28] Phosphine oxides are also increasingly being used in medicinal chemistry; the drug brigatinib features a dimethylphosphine oxide group that functions as an important H-bond acceptor, imparting favorable pharmacokinetic properties on the molecule relative to other commonly used polar groups.[29] Arsine oxides are generally similar to phosphine oxides in both structure and reactivity, but are more basic and prone to reduction.[30–32]

The pK_{aH} values of triphenylphosphine oxide and triphenylarsine oxide in water have been reported as −2.10 and 0.99, respectively.[32] To the best of our knowledge, the only series that has been extended to include antimony comprises trimethylphosphine oxide, trimethylarsine oxide, and trimethylstibine oxide, the pK_{aH} values of which were reported to be 0, 3.75, and 5.36, respectively, following an increasing trend in basicity as the pnictogen becomes heavier.[32,33] Recent studies strongly suggests, however, that a stibine oxide with substituents as small as those of trimethylstibine oxide would actually exist as a dimeric or oligomeric species.[34,35] In such a case, the apparent basicity of the stiboryl group would be dramatically attenuated. The Brønsted basicity of phosphine oxides has been studied *via* their interactions with phenols, which can complex with phosphine oxides to form isolable H-bonded adducts.[36–40] Proton transfer from substituted phenols to triphenylphosphine oxide was assessed by monitoring the deshielding of relevant nuclei using solution and solid-state NMR spectroscopy.[38] In general, decreases in pK_a of the phenol were correlated to increased proton transfer to triphenylphosphine oxide, but intramolecular H-bonding and steric effects can obscure these trends. Whereas phenols co-crystallize with triphenylphosphine oxide to form H-bonded adducts (O–H···O), stronger acids can formally protonate the phosphoryl group to form hydroxyphosphonium salts ($X^-\cdots{}^+H$–O) in the solid state.[41] The location of a species on the salt–co-crystal continuum requires careful attention and we recently demonstrated that previous reports of monomeric stibine oxides engaged in H-bonding interactions were in fact hydroxystibonium salts.[42,43] Recent developments in Hirshfeld atom refinement show great promise in aiding researchers in this regard.[44,45]

The utility of phosphine oxides comes from the remarkable stability and polarity of the phosphoryl bond. The unique bonding situation that gives rise to such properties was hotly debated for decades. Although the apparent multiple-bonding character of the phosphoryl group was initially thought to arise from delocalization of O-centered lone pairs into d orbitals centered on the P atom,[46,47] these orbitals are now known to be too high in energy to participate in the P–O bonding interaction. Instead, the spatially and energetically accessible P–C σ* orbitals accept electron density from the O-centered lone pairs (Fig. 1). A series of topological analyses on amine, phosphine, and arsine oxides within the framework of Bader's Quantum Theory of Atoms in Molecules (QTAIM) revealed that the ellipticity was 0 for each at the Pn–O bond critical point (bcp), which indicates the presence of a cylindrically symmetrical bonding interaction.[48,49] In phosphine oxides, three

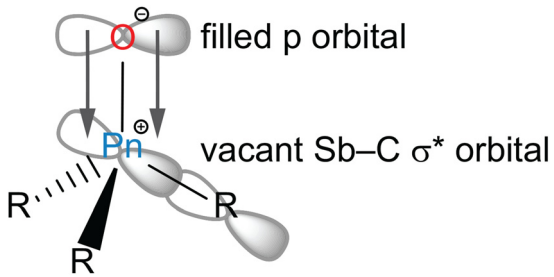

Fig. 1 Accepted model for pnictoryl bonding featuring a polar covalent single bond between the Pn and O atoms and dative interactions between the O-centered, p-hybridized lone pairs and Pn–C σ* acceptor orbitals (Pn = P, As, Sb).

valence-shell charge concentrations (minima in the Laplacian) corresponding to three O-centered lone pairs were arrayed in a staggered configuration relative to the three P–X bonds. Although the extent of back-bonding to the P–C σ* orbitals was not quantified, these analyses led the authors to conclude that the bonding interaction is a highly polarized covalent single bond (P^+–O^-). The presence of strong back-bonding interactions was subsequently confirmed by analysis of the QTAIM delocalization index and electron localization function.[50,51] Recently, energy decomposition analysis further supported the description of the phosphoryl bond as a polar covalent single-bond stabilized by electrostatic interactions and delocalization from the O-centered lone pairs to the P–C σ* antibonding orbitals.[52]

These descriptions of the nature of the phosphoryl bond indicate that replacement of the P atom with a heavier pnictogen will have a significant impact on the electronic structure of these molecules and, consequently, their reactivity. Increase in the size and diffuseness of the pnictogen valence orbitals and increase in the Pn–O bond length should both result in a reduction of overlap between the O-centered lone pairs and the Pn–C σ* orbitals, disrupting back-donation. Furthermore, an increasing difference in electronegativity between the O and Pn atoms as the group is descended should favor a greater separation of charge across the Pn–O bond. Until very recently, experimental verification of these expected trends was limited by the fact that monomeric pnictine oxides exhibiting unperturbed pnictoryl groups were only known for phosphorus and arsenic. We recently succeeded in preparing the first unperturbed monomeric stibine oxide, $Dipp_3SbO$ (where Dipp = 2,6-diisopropylphenyl) (**1a**), by capitalizing on the kinetic stabilization afforded by the bulky aryl substituents (Scheme 1).[53] We also isolated its lighter congeners $Dipp_3AsO$ (**1b**) and $Dipp_3PO$ (**1c**) for direct comparison. We note that monomeric bismuthine oxides are an unknown class of molecule, preventing the extension of periodic trends in pnictoryl bonding to bismuth.

Herein, we quantitatively describe the impact that the variation in electronic structure across the series of monomeric pnictine oxides **1a–c** has on their Brønsted basicity. We first discuss a theoretical investigation into proton affinity and

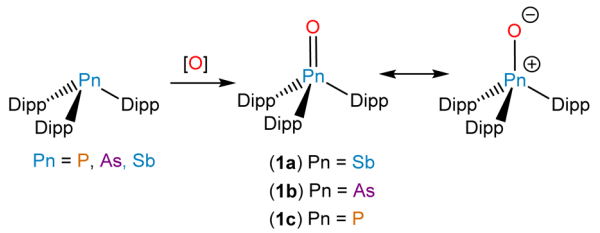

Scheme 1 Synthesis of monomeric pnictine oxides. Oxidation of $Dipp_3Pn$ yields monomeric $Dipp_3PnO$ for Pn = P (**1c**), As (**1b**), and Sb (**1a**). $Dipp_3P$ and $Dipp_3As$ are oxidized by *m*CPBA; $Dipp_3Sb$ is oxidized by iodosobenzene.

acid–base thermochemistry of the pnictine oxides with a series of substituted phenols. We then explore the acid–base chemistry of **1a–c** in solution and in the solid state with a series of Brønsted acids of varied strength. NMR spectroscopic monitoring of the titration of hydroxypnictonium triflate salts with appropriate bases allowed for pK_{aH} determination of **1a–b**. We then compare catalytic efficiencies of **1a–c** in a Brønsted base-catalyzed transesterification reaction. Our results unambiguously demonstrate the stark increase in Brønsted basicity as the pnictogen becomes heavier from **1c** < **1b** < **1a**.

Results and discussion

Theoretical investigation of basicity

We previously performed a detailed theoretical investigation of **1a–c** (DKH-PBE0/old-DKH-TZVPP//PBE0/def2-TZVPP); select results are reproduced in Table 1.[53] To facilitate the subsequent discussion, we briefly recapitulate some of the findings from that prior work. Topological analysis revealed a bond critical point on each Pn–O interatomic vector. The magnitude of ρ_{bcp} systematically decreases from **1c** > **1b** > **1a**. The HOMOs exhibit large contributions from O-centered lone pairs and are less stabilized as the pnictogen becomes heavier. The LUMO of **1a** is the most energetically accessible and has predominant σ*(Pn–O) character, consistent with prior reports of high Lewis acidity at pentavalent antimony.[54] In agreement with our analysis of the canonical molecular orbitals, the natural charge on the O atom becomes increasingly negative as the pnictogen becomes heavier, and the natural charge on the pnictogen is the highest in the case of **1a**. Furthermore, the energy of destabilization upon deletion of all dative interactions between the O and $Dipp_3Pn$ fragments systematically decreases from **1c** > **1b** > **1a**. These results are consistent with the aforementioned electronic structure: as the pnictogen atom increases in atomic number, σ bonding weakens and π-backdonation from the O-centered lone pairs to the Pn–C σ* orbitals is disrupted, polarizing and weakening the pnictoryl bond. The consequent buildup of charge on the O-atom suggests that both Brønsted and Lewis basicity will increase from **1c** < **1b** < **1a**. Our preliminary investigation into the reactivity of these species with Brønsted acids confirmed this hypothesis.[53] We previously observed that addition of 1 equiv of benzenesulfonic acid to **1a** or **1b** cleanly affords the hydroxypnictonium benzenesulfonate salts. In the case of **1c**, titration with excess benzenesulfonic acid was needed to observe the formation of hydroxyphosphonium in solution. In the case of **1a**, a 1 : 1 mixture of the stibine oxide and acetic acid cleanly afforded the *cis*-hydroxyacetatostiborane; no such reaction was observed with either **1b** or **1c**.

To begin our systematic evaluation of the Brønsted basicity of **1a–c**, we calculated the theoretical gas-phase proton affinities of the pnictine oxides; they increase from **1c** < **1b** < **1a** (Table 2). Isodesmic reaction free energies were calculated for the protonations of **1a–c** with substituted phenols (Table 2). Our calculations indicate that reactions between either **1a** or **1b** with picric acid would readily yield the corresponding hydroxypnictonium salts and that no reaction with **1c**

Table 2 Calculated proton affinities of **1a–c**[a,b]

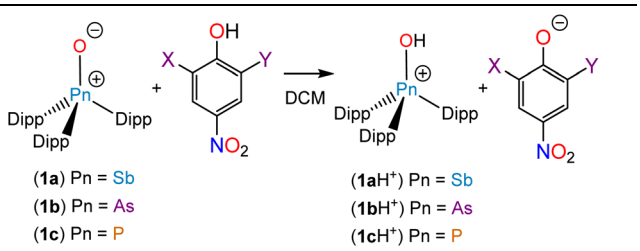

	PA	ΔG (i)	ΔG (ii)	ΔG (iii)
1a	266	−16.9	−7.9	−3.4
1b	253	−5.45	4.0	8.0
1c	239	7.7	16.7	21.2

[a] Proton affinities (PA) and isodesmic reaction free energies calculated at the PBE0/def2-TZVPP level of theory. Units are kcal mol^{-1}. [b] (i) X = Y = NO_2, (ii) X = H, Y = NO_2, (iii) X = Y = H.

Table 1 Select properties of **1a–c** calculated at the DKH-PBE0/old-DKH-TZVPP//PBE0/def2-TZVPP level of theory[a]

	ρ_{bcp} (Pn–O)[b] (e^- Å^3)	Pn HOMO[c] (eV)	Pn LUMO[d] (eV)	NPA O[e] (e^-)	NPA Pn[f] (e^-)	E_{def}[g] (kcal mol^{-1})
1a	0.173	−6.29	−0.82	−1.24	2.16	92
1b	0.216	−6.55	−0.72	−1.14	1.84	117
1c	0.232	−6.77	−0.79	−1.13	1.91	172

[a] These values are reproduced from a prior report.[53] [b] Electron density at the Pn–O bond critical point. [c] Energy of HOMO. [d] Energy of LUMO. [e] Natural charge of the O atom. [f] Natural charge of the pnictogen atom. [g] Energy of destabilization upon deletion of dative interactions between the O atom and $Dipp_3Pn$ molecular fragments.

would be observed. Protonation of **1a–c** with 2,4-dinitrophenol was predicted to be favorable only in the case of **1a**. Protonation of **1a** by *p*-nitrophenol was predicted to be favorable, albeit by only a small margin.

Reactions with triflic acid

We next combined **1a–c** with acids of varying strengths to evaluate their relative Brønsted basicities experimentally (Scheme 2). The NMR spectra of **1a–c** feature two distinct benzylic proton resonances due to restricted rotation about the Sb–C_{ipso} bond such that there is a relatively deshielded Pn-proximal proton and a relatively shielded O-proximal benzylic proton. The benzylic resonances appear in an unobscured region of the spectrum and exhibit dramatic changes upon chemical manipulation, thus they serve as convenient reporters for the extent of H-bonding between **1a–c** and Brønsted acids. Addition of triflic acid to solutions of **1a–c** results in dramatic shifts of the benzylic proton signals, as seen in the ^{1}H NMR spectra (see Fig. S15†), consistent with formation of hydroxypnictonium triflate salts **2a–c**.[53] In the ^{31}P NMR spectrum of a mixture of **1c** and triflic acid, a single broad signal is observed at 50.60 ppm, which is shifted significantly downfield from that of free **1c** (25.33 ppm), further consistent with formation of the hydroxyphosphonium cation. The hydroxystibonium triflate (**2a**) crystallized preparatively from a mixture of DCM and hexanes. Single-crystal X-ray diffraction showed the crystals to have formed in space group $P\bar{1}$ (Fig. 2A). The Sb–O

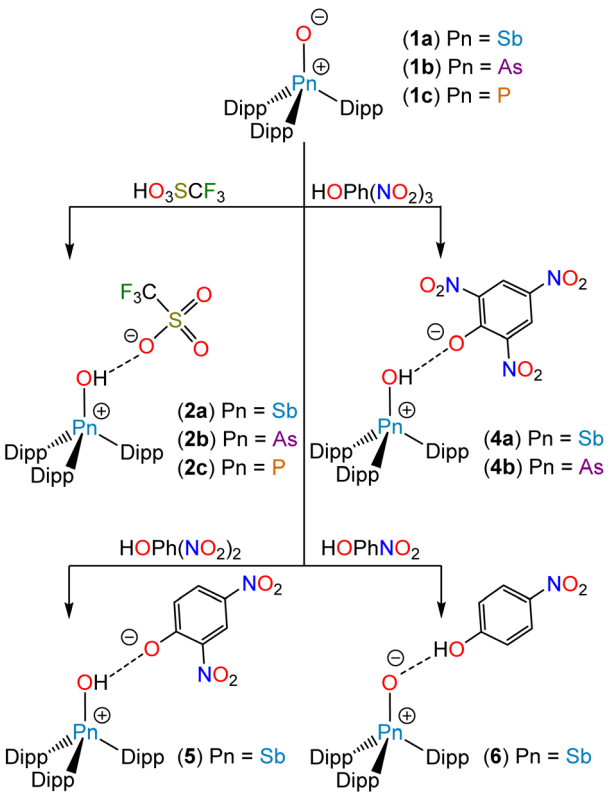

Scheme 2 Reactions between **1a–c** and acids to form **2a–c**, **4a–b**, **5**, and **6**.

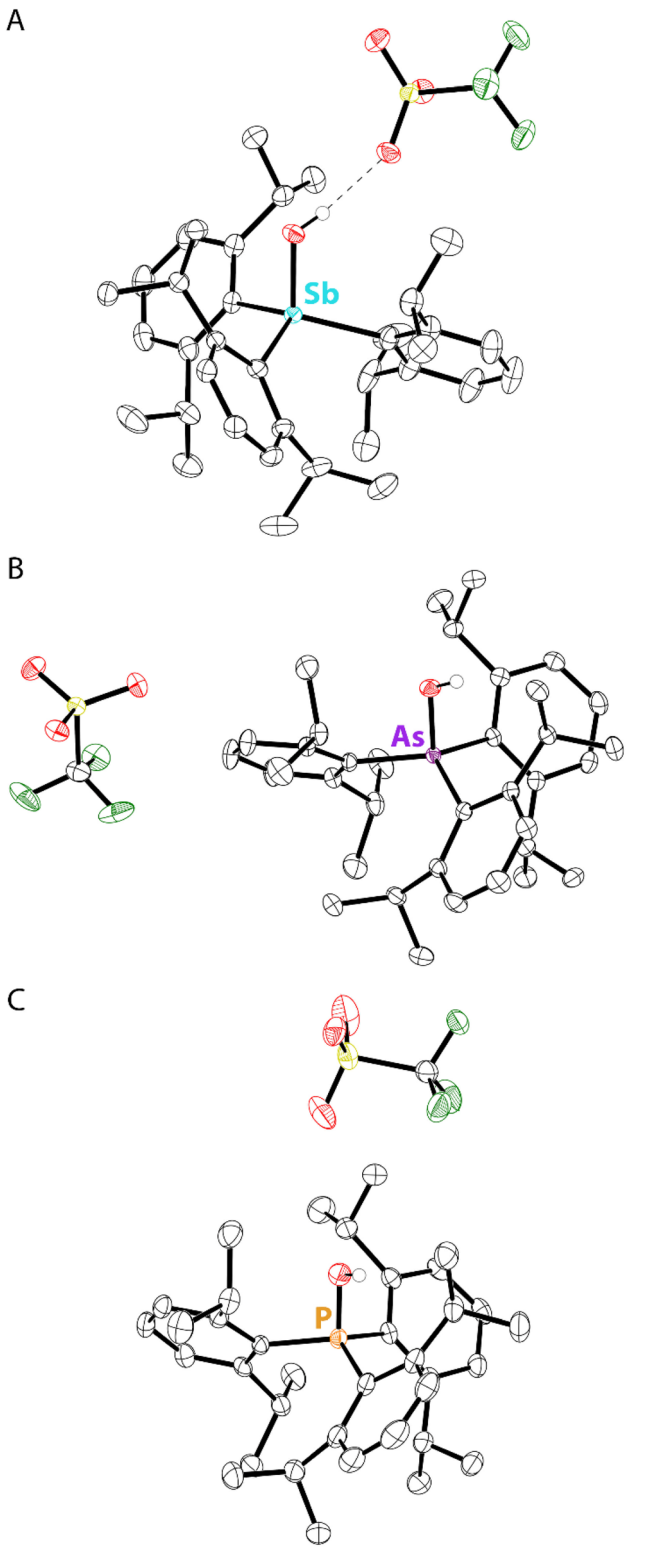

Fig. 2 Thermal ellipsoid plots (50% probability) of (A) **2a**, (B) **2b** triclinic, and (C) **2c**. Color code: Sb teal, As purple, P orange, O red, C black, S yellow, F green, and H grey spheres of arbitrary radius. C-bound H atoms and solvent molecules are omitted for clarity.

bond length was 1.9198(12) Å, significantly longer than that of **1a** (1.8428(14) Å) and characteristic of a hydroxystibonium species.[42,43,53,55] The triflate counteranion of **2a** engages with the protic H atom as an H-bond acceptor.

Vapor diffusion of pentane into a chloroform solution of **1b** and triflic acid resulted in the preparative formation of colorless crystals but microscopic inspection revealed the presence of two distinct crystal habits. The majority of the material appeared as blocks, but there was also a small number of needles present. Single-crystal X-ray diffractometric experiments with a representative individual from each set of crystals revealed them to be polymorphs of **2b**·$CHCl_3$. The blocks and needles belonged to the triclinic and monoclinic crystal families, respectively. A notable difference between the polymorphs is the position of the triflate anion. In the triclinic polymorph, the triflate counteranion is free from the hydroxyarsonium cation and only acts as an H-bond acceptor for a $CHCl_3$ molecule (Fig. 2B). In the monoclinic polymorph, the triflate anion engages both the hydroxyl group and the solvent molecule in H-bonding interactions.

We note that slow evaporation of a DCM/pentane solution of **1c** and triflic acid afforded colorless crystals; however, these crystals were highly unstable. The material rapidly decomposed to an unknown mixture of compounds on contact with Paratone oil, but rapid manipulation and subsequent immersion into a stream of 100 K N_2 allowed the structure of these crystals to be successfully determined by X-ray diffraction methods. The crystals were found to be the hydroxyphosphonium triflate **2c**, where the triflate anion does not hydrogen bond with the hydroxyl group (Fig. 2C). The structures of the **2a–c** series exhibit a systematic trend whereby interaction of the triflate anion with the hydroxypnictonium cation is present in **2a**, variable in **2b**, and absent in **2c**. As described above, the basicity of the pnictine oxides increases from **1c** to **1b** to **1a**, and the stabilities of the conjugate acids increase similarly. Analysis of the geometries of the computationally optimized structures of the conjugate acids (*vide supra*) shows that the calculated O–H bond lengths are nearly identical at 0.963, 0.962, and 0.961 Å for **1c**H^+, **1b**H^+, and **1a**H^+, respectively. The theoretically calculated positive charge on the protic H atom in these complexes similarly shows a small, albeit more pronounced, systematic variation from 0.54 to 0.51 to 0.50 for **1c**H^+, **1b**H^+, and **1a**H^+, respectively. These trends would appear to suggest that the propensity of the hydroxypnictonium cation to engage in an electrostatic H-bonding interaction with triflate would increase from **1a**H^+ to **1c**H^+, which is the opposite of the trend exhibited by the crystal structures. We believe that the more significant structural variation is that in the Pn–OH bond length: 1.592, 1.751, and 1.934 Å for **1c**H^+, **1b**H^+, and **1a**H^+, respectively. The hydroxyl group of the hydroxyphosphonium is simply too buried within the pocket of the Dipp groups to engage with the triflate. Space-filling diagrams of **1a–c**H^+ demonstrate the increased steric crowding present in **1c**H^+ that we suggest is primarily responsible for attenuating interaction with the counterion (Fig. S61†). In addition to this steric hindrance, the sterically enforced proximity of the protic and benzylic H atoms results in intramolecular dihydrogen bonding (see ESI†), which could further attenuate the capacity of the P–OH group to engage in interactions with the counterion. In one instance, a small portion of crystals grown from a mixture of **1c** and triflic acid was shown by X-ray crystallography to be composed not of **2c**, but rather the cyclized alkoxyphosphonium triflate salt **3** (see ESI for discussion†).

Reactions with substituted phenols

Returning to the reactions computationally investigated in Scheme 2, we proceeded to experimentally investigate less acidic proton donors. Addition of picric acid to solutions of **1a** and **1b** resulted in dramatic shifts of the benzylic proton resonances, but a similar effect was not observed in the case of **1c**. Vapor diffusion of pentane into a chloroform solution of **1a** and picric acid yielded bright yellow crystals of hydroxystibonium picrate (**4a**) (Fig. 3A). Layering a bright yellow chloroform solution of **1b** and picric acid under cyclohexane resulted in the preparative growth of yellow crystals, which X-ray diffrac-

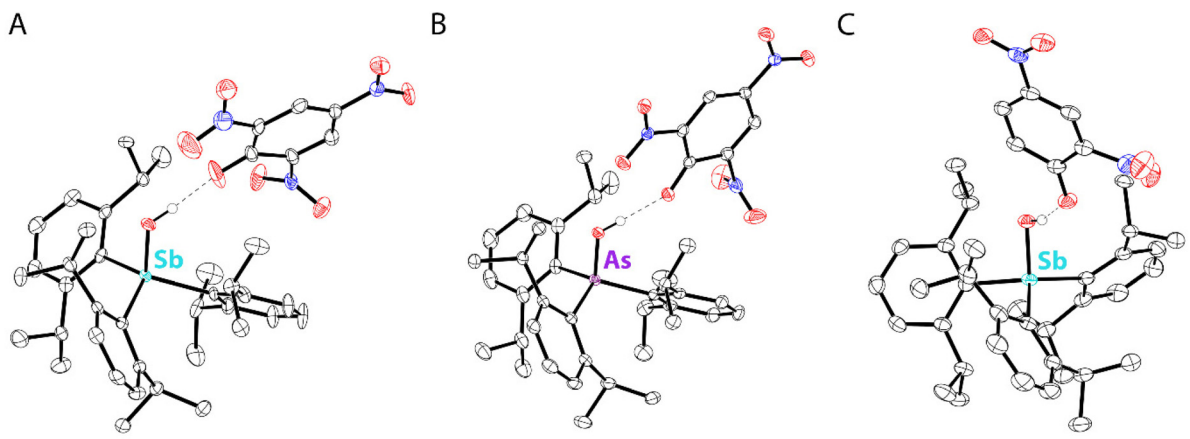

Fig. 3 Thermal ellipsoid plots (50% probability) of (A) **4a**, (B) **4b**, (C) **5**. Color code: Sb teal, As purple O red, N blue, C black, H grey spheres of arbitrary radius. C-bound H atoms and solvent molecules are omitted for clarity.

tion revealed to be the hydroxyarsonium picrate cyclohexane solvate (**4b**·$\frac{3}{4}$(C_6H_{12})) (Fig. 3B). Attempts to isolate H-bonded adducts between picric acid and **1c** were unsuccessful, consistent with the lack of observed interaction by NMR spectroscopy. Considering that an H-bonded adduct between triphenylphosphine oxide and the even weaker proton donor *p*-nitrophenol has been isolated,[36,38] we propose that steric shielding may make such interactions unfavorable in the present system.

The reaction between 2,4-dinitrophenol and **1a** behaved similarly to that between **1a** and picric acid: dramatic shifts in the benzylic proton resonances indicate that protonation of the stiboryl group occurs. A preparative yield of bright yellow crystals of **5**·2($CHCl_3$) was obtained by layering a chloroform solution of **1a** and 2,4-dinitrophenol under cyclohexane (Fig. 3C). In agreement with our calculated reaction free energies (Table 2), no similar reaction was observed by combining either **1b** or **1c** with 2,4-dinitrophenol, experimentally confirming the drastic decrease in the Brønsted basicity of **1c** and **1b** as compared to **1a**. Attempts to isolate an H-bonded adduct between either **1c** or **1b** and 2,4-dinitrophenol were unsuccessful.

Addition of an equivalent of *p*-nitrophenol to a solution of **1a** did not result in the large shift of the benzylic resonances that was observed upon addition of the stronger acids, as described above. However, vapor diffusion of pentane into a 1 : 1 mixture of *p*-nitrophenol and **1a** in chloroform resulted in the growth of yellow crystals (**6**). Dissolution of **6** yielded a solution whose NMR spectrum indicated the presence of a 1 : 1 mixture of the phenol and **1a**. The benzylic resonances of **1a** appeared only slightly shifted and sharpened, consistent with a weak interaction between the two species. The crystal structure of **6** reveals **1a** and *p*-nitrophenol in the asymmetric unit, with the stiboryl and phenolic O atoms at a distance of 2.449(1) Å, consistent with an H-bonding interaction (Fig. 4A). The Sb–O bond was measured at 1.8627(9) Å, shorter than a hydroxystibonium and consistent with Lewis acid-coordinated stibine oxides.[42,43,53] The protic H atom was located in the Fourier difference map, and its position and isotropic thermal parameters were refined freely using Hirshfeld atom refinement to afford O_{phenol}–H and O_{1a}···H distances of 1.14(3) and 1.32(3) Å, respectively. These data strongly suggest that **6** is an H-bonded adduct between **1a** and *p*-nitrophenol, as opposed to a hydroxystibonium phenoxide salt. Interestingly, if pentane was allowed to diffuse into a 2 : 1 mixture of *p*-nitrophenol and **1a**, a second equivalent of *p*-nitrophenol crystallizes in the asymmetric unit. The structure, determined by Hirshfeld atom refinement, contains a phenoxide anion engaged in H-bonding interactions with both a hydroxystibonium cation and a *p*-nitrophenol molecule (Fig. 4B). The second equivalent of *p*-nitrophenol stabilizes the phenoxide O-atom such that the proton migrates to the stiboryl O atom and formally forms a hydroxystibonium salt. In this case, the Sb–O bond length is 1.9026(7) Å and the $O_{phenoxide}$···H and O_{1a}–H distances are 1.53(2) and 1.03(2) Å, respectively. These structures indicate that *p*-nitrophenoxide and **1a** are close in Brønsted basicity, with *p*-nitrophenoxide being the slightly stronger base.

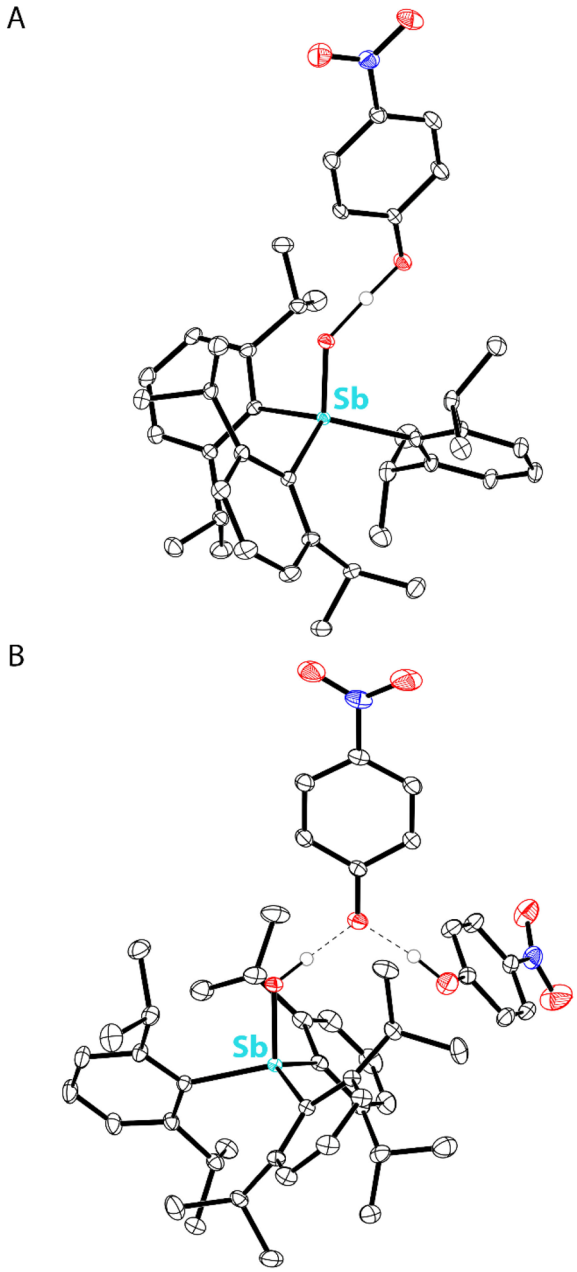

Fig. 4 Thermal ellipsoid plots (50% probability) of (A) **6**, (B) **6**·*p*-nitrophenol. Color code: Sb teal, O red, N blue, C black, H grey spheres of arbitrary radius. C-bound H atoms are omitted for clarity.

Determination of stibine oxide pK_a

The stoichiometric reactivity described above is consistent with our prediction of the significantly enhanced basicity of **1a** as compared to **1b** and **1c**. pK_{aH} values have previously been determined for triphenyl- and trimethyl-substituted phosphine oxides and arsine oxides, and they show increases of 3–4 on proceeding from an R_3PO species to the analogous R_3AsO.[32] The prior absence of available monomeric stibine oxides prevented an extension of this trend. The reactivity with the nitro-substituted phenols suggests that the p$K_{aH,MeCN}$ of the stibine

oxide **1a** would lie between that of 2,4-dinitrophenol ($pK_{a,MeCN}$ = 16.66) and *p*-nitrophenol ($pK_{a,MeCN}$ = 20.7).[56] We measured the $pK_{aH,MeCN}$ of **1a** by performing NMR spectrometric titrations in acetonitrile-d_3 (Fig. 5A). The dramatic shift in the Pn-proximal benzylic ^{1}H NMR resonances upon protonation of **1a** makes these signals a convenient spectroscopic handle to follow during titration. Our initial estimate of the $pK_{aH,MeCN}$ from the nitrophenol reactivity suggested that titration of **2a** with the sterically bulky base Et_3N ($pK_{aH,MeCN}$ = 18.83)[57] would allow the needed equilibria to be established. The salt **2a** was chosen because the weakly coordinating triflate anion prevents other strong H-bonding interactions from convoluting the data. Indeed, we observed that increasing concentrations of Et_3N resulted in a systematic conversion of **2a** into **1a**. The observed chemical shift of the benzylic protons results from the weighted average of the relative populations of the protonated and deprotonated species, and the extracted concentrations of each species in solution were analyzed as a function of added base to determine that the $pK_{aH,MeCN}$ of **1a** is 19.81 (5), where the error reflects the standard deviation of the $pK_{aH,MeCN}$ values from three independently performed titrations (Fig. 5B).

For the sake of direct comparison and to validate our methodology, we similarly determined the $pK_{aH,MeCN}$ of **1b** (Fig. 5C). From the nitrophenol reactivity, we anticipated that the value would fall between that of picric acid ($pK_{a,MeCN}$ = 11.00) and 2,4-dinitrophenol ($pK_{a,MeCN}$ = 16.66). We consequently chose the bulky base acridine as the titrant ($pK_{aH,MeCN}$

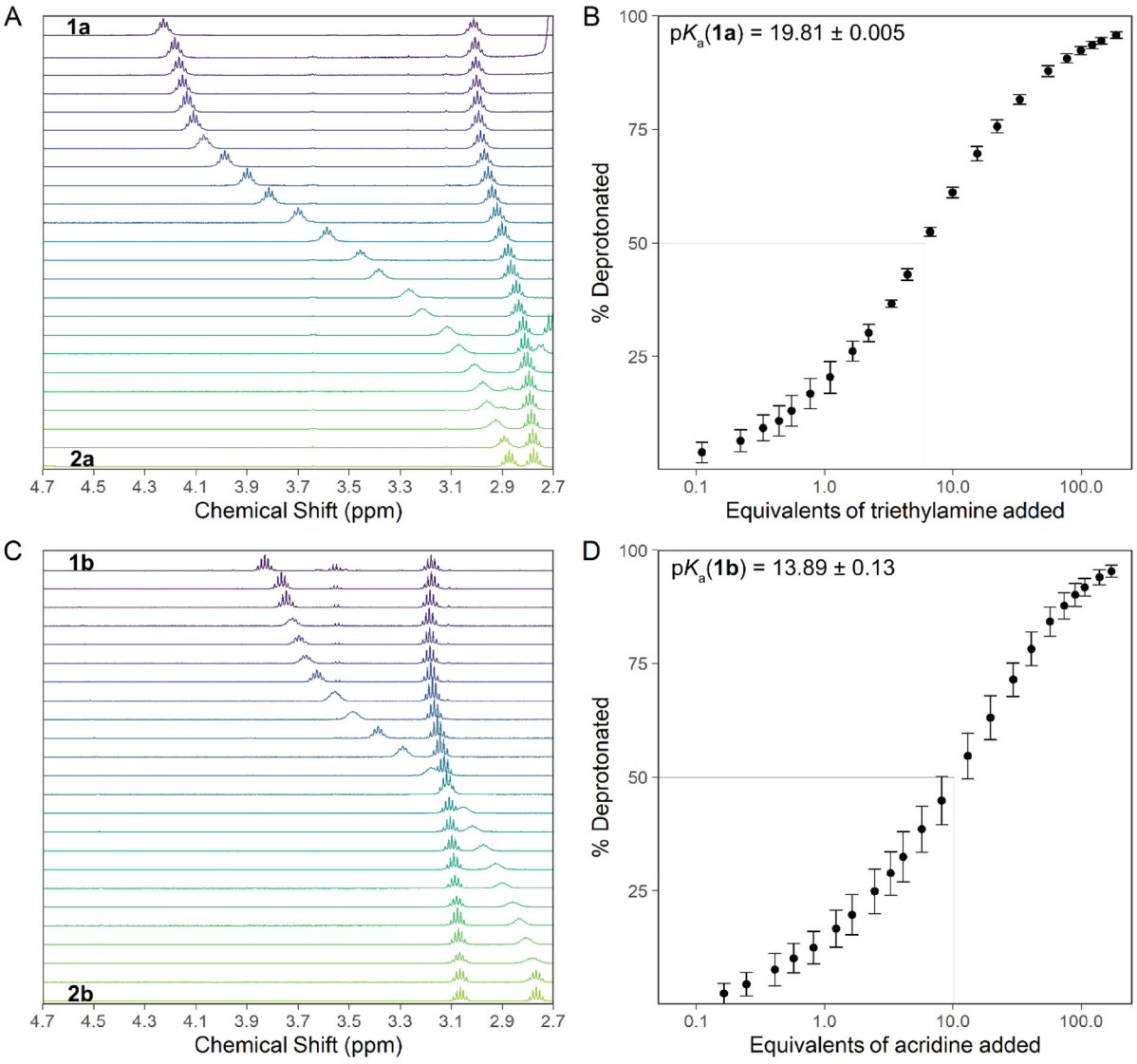

Fig. 5 Left: Stacked ^{1}H NMR spectra used to determine pK_{aH} of (A) **1a** and (C) **1b**. The bottom spectrum is of a solution of only hydroxypnictonium triflate and the top spectrum is of a solution of only pnictine oxide. Intervening spectra are of samples with increasing concentration of titrant from bottom to top (see ESI for numerical data†). Right: Averaged data that were fit to determine the pK_{aH} of (B) **1a** and (D) **1b**. Error bars reflect the standard deviation of three independent replicates.

= 12.16)[57] for **2b**, with the triflate salt of the hydroxypnictonium cation being chosen for the same reason as above. The $pK_{aH,MeCN}$ of **1b** was 13.89(13) (Fig. 5D). These pK_a values allow us to quantitatively compare the pnictine oxide basicities. The increase of basicity from **1b** to **1a** agrees with the increase previously observed from phosphine oxide to arsine oxide, but is orders of magnitude greater; whereas arsine oxides are typically 1000-fold stronger bases than phosphine oxides,[32,33] the stibine oxide **1a** is 10^6-fold more basic than the arsine oxide **1b**.

Brønsted base catalysis

Among their many demonstrated applications, the basicity of pnictine oxides has allowed them to serve as Brønsted bases in either a stoichiometric or catalytic fashion. The nearly million-fold increase of basicity from the arsine oxide **1b** to the stibine oxide **1a** suggested to us that the latter could be able to function as an enhanced Brønsted base catalyst as compared to the lighter congeners. To demonstrate this capability, we targeted the synthesis of 2,2,2-trifluoroethyl acetate. 2,2,2-Trifluoroethyl esters are moderately activated and can react cleanly with primary amines to form amides without the need for a coupling reagent.[58,59] Transesterification between *p*-nitrophenyl acetate and 2,2,2-trifluoroethanol to form *p*-nitrophenol and 2,2,2-trifluoroethyl acetate reached 97% completeness in the presence of 20 mol% of **1a** within 26 h at 50 °C in chloroform-*d* (Table 3). Under similar conditions, **1b** only reached 13% completion and **1c** showed no catalytic activity. NMR spectroscopic measurements acquired during reactions catalyzed by **1a** show only signals for the $[Dipp_3Sb(OH)]^+$ cation (Fig. S35†); those catalyzed by **1b** showed a mixture of $[Dipp_3As(OH)]^+$ and $Dipp_3AsO$ (Fig. S37†); those performed with **1c** showed only $Dipp_3PO$ (Fig. S39†). This observed reactivity is consistent with Brønsted base catalysis and we propose that steric crowding precludes catalytic activity at the Lewis acidic Pn atoms. We emphasize that this reactivity was explored to illustrate the difference in reactivity across the series; the exploration of practical uses of this chemistry is actively underway.

Table 3 Transesterification between *p*-nitrophenyl acetate and 2,2,2-trifluoroethanol (TFE)

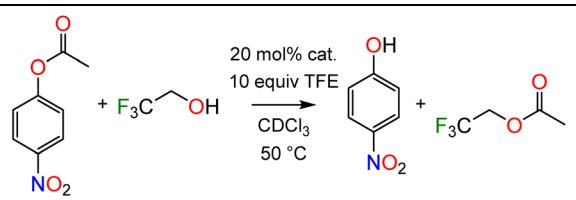

Catalyst	% Conversion
1a	97
1b	13
1c	0
None	0

Conclusion

The systematic variation in electronic structure of the pnictoryl Pn^+–O^- bond from previously known phosphine oxides and arsine oxides to the newly available monomeric stibine oxide has a direct impact on the Brønsted basicities of these species. Notably, the decrease in donation from the oxygen lone pairs into Pn–C σ* orbitals as the pnictogen becomes heavier results in a dramatic increase in basicity for the stibine oxide. Here we have theoretically predicted this increase and demonstrated its magnitude through stoichiometric reactivity with acids of varying strength. The results of that stoichiometric reactivity were used to design spectrometric titrations that have permitted the first determination of the $pK_{aH,MeCN}$ of a monomeric stibine oxide. This value, when compared to those of the lighter congeners, provides insight, for the first time, into the enhanced basicity of the stiboryl group. We also demonstrate that this increased basicity can be exploited to enhance pnictine oxide-catalyzed reactions. We are continuing to explore the basicity of these species, alternative reactivity of the newly accessible stibine oxide functional group, and the stabilization of other unsaturated main-group motifs.

Data availability

Crystallographic data for **2a**, **2b** (monoclinic), **2b** (triclinic), **2c**, **3**, **4a**, **4b**, **5**, **6**·*p*-nitrophenol, and **6** have been deposited at the Cambridge Crystallographic Data Centre, under deposition numbers CCDC 2250578–2250587, and can be obtained from https://www.ccdc.cam.ac.uk/structures/.† Source data used to generate the plots in Fig. 5 are available in Tables S5–S10 of the ESI† PDF document. Full experimental details, NMR spectra, IR spectra, and Cartesian coordinates of computationally optimized molecular geometries are also available in the ESI PDF document.†

Author contributions

J. S. W. and A. G. performed experiments, J. S. W., A. G., and T. C. J. analyzed data, and J. S. W. and T. C. J. wrote the manuscript.

Conflicts of interest

There are no conflicts to declare.

Acknowledgements

The single-crystal X-ray diffractometer housed in the UCSC X-ray Diffraction Facility was funded by NSF MRI grant 2018501 and this work was further supported by the NSF through a CAREER award 2236365 to T. C. J.

References

1 D. You and F. P. Gabbaï, *Trends Chem.*, 2019, **1**, 485–496.
2 E. Rivard and P. P. Power, *Inorg. Chem.*, 2007, **46**, 10047–10064.
3 P. P. Power, *Nature*, 2010, **463**, 171–177.
4 V. Nesterov, D. Reiter, P. Bag, P. Frisch, R. Holzner, A. Porzelt and S. Inoue, *Chem. Rev.*, 2018, **118**, 9678–9842.
5 R. J. Gilliard and C.-W. Chiu, *Organometallics*, 2020, **39**, 4123–4126.
6 J. M. Lipshultz, G. Li and A. T. Radosevich, *J. Am. Chem. Soc.*, 2021, **143**, 1699–1721.
7 C. J. O'Brien, J. L. Tellez, Z. S. Nixon, L. J. Kang, A. L. Carter, S. R. Kunkel, K. C. Przeworski and G. A. Chass, *Angew. Chem., Int. Ed. Engl.*, 2009, **48**, 6836–6839.
8 S. Lim and A. T. Radosevich, *J. Am. Chem. Soc.*, 2020, **142**, 16188–16193.
9 N. L. Dunn, M. Ha and A. T. Radosevich, *J. Am. Chem. Soc.*, 2012, **134**, 11330–11333.
10 W. Zhao, S. M. McCarthy, T. Y. Lai, H. P. Yennawar and A. T. Radosevich, *J. Am. Chem. Soc.*, 2014, **136**, 17634–17644.
11 C. Lichtenberg, *Chem. Commun.*, 2021, **57**, 4483–4495.
12 F. Wang, O. Planas and J. Cornella, *J. Am. Chem. Soc.*, 2019, **141**, 4235–4240.
13 Y. Pang, M. Leutzsch, N. Nöthling and J. Cornella, *J. Am. Chem. Soc.*, 2020, **142**, 19473–19479.
14 O. Planas, F. Wang, M. Leutzsch and J. Cornella, *Science*, 2020, **367**, 313–317.
15 Y. Pang, M. Leutzsch, N. Nöthling, F. Katzenburg and J. Cornella, *J. Am. Chem. Soc.*, 2021, **143**, 12487–12493.
16 H. W. Moon and J. Cornella, *ACS Catal.*, 2022, **12**, 1382–1393.
17 M. B. Kindervater, K. M. Marczenko, U. Werner-Zwanziger and S. S. Chitnis, *Angew. Chem., Int. Ed. Engl.*, 2019, **58**, 7850–7855.
18 T. Hynes, J. D. Masuda and S. S. Chitnis, *ChemPlusChem*, 2022, e202200244.
19 G. Wittig and U. Schöllkopf, *Chem. Ber.*, 1954, **87**, 1318–1330.
20 O. Mitsunobu and M. Yamada, *Bull. Chem. Soc. Jpn.*, 1967, **40**, 2380–2382.
21 R. Appel, *Angew. Chem., Int. Ed. Engl.*, 1975, **14**, 801–811.
22 H. Staudinger and J. Meyer, *Helv. Chim. Acta*, 1919, **2**, 635–646.
23 S. Kotani and M. Nakajima, *Tetrahedron Lett.*, 2020, **61**, 151421.
24 H. Morimoto, T. Yoshino, T. Yukawa, G. Lu, S. Matsunaga and M. Shibasaki, *Angew. Chem., Int. Ed.*, 2008, **47**, 9125–9129.
25 R. Yazaki, N. Kumagai and M. Shibasaki, *J. Am. Chem. Soc.*, 2010, **132**, 5522–5531.
26 B. Shankar, P. Elumalai, R. Shanmugam, V. Singh, D. T. Masram and M. Sathiyendiran, *Inorg. Chem.*, 2013, **52**, 10217–10219.
27 M. Keener, C. Hunt, T. G. Carroll, V. Kampel, R. Dobrovetsky, T. W. Hayton and G. Ménard, *Nature*, 2020, **577**, 652–655.
28 M. A. Beckett, G. C. Strickland, J. R. Holland and K. S. Varma, *Polymer*, 1996, **37**, 4629–4631.
29 W.-S. Huang, S. Liu, D. Zou, M. Thomas, Y. Wang, T. Zhou, J. Romero, A. Kohlmann, F. Li, J. Qi, L. Cai, T. A. Dwight, Y. Xu, R. Xu, R. Dodd, A. Toms, L. Parillon, X. Lu, R. Anjum, S. Zhang, F. Wang, J. Keats, S. D. Wardwell, Y. Ning, Q. Xu, L. E. Moran, Q. K. Mohemmad, H. G. Jang, T. Clackson, N. I. Narasimhan, V. M. Rivera, X. Zhu, D. Dalgarno and W. C. Shakespeare, *J. Med. Chem.*, 2016, **59**, 4948–4964.
30 T. Nemoto, T. Ohshima, K. Yamaguchi and M. Shibasaki, *J. Am. Chem. Soc.*, 2001, **123**, 2725–2732.
31 D. Phillips and S. Tyree Jr., *J. Am. Chem. Soc.*, 1961, **83**, 1806–1810.
32 C. Klofutar, F. Krašovec and M. Kušar, *Croat. Chem. Acta*, 1968, **40**, 23–28.
33 P. Nylén, *Z. Anorg. Allg. Chem.*, 1941, **246**, 227–242.
34 J. Bordner, G. O. Doak and T. S. Everett, *J. Am. Chem. Soc.*, 1986, **108**, 4206–4213.
35 C. J. Carmalt, J. G. Crossley, N. C. Norman and A. G. Orpen, *Chem. Commun.*, 1996, 1675–1676.
36 R. M. Fuquen and J. R. Lechat, *Acta Crystallogr., Sect. C: Cryst. Struct. Commun.*, 1992, **48**, 1690–1692.
37 R. Cuypers, B. Burghoff, A. T. M. Marcelis, E. J. R. Sudhölter, A. B. De Haan and H. Zuilhof, *J. Phys. Chem. A*, 2008, **112**, 11714–11723.
38 C. M. Lagier, U. Scheler, G. McGeorge, M. G. Sierra, A. C. Olivieri and R. K. Harris, *J. Chem. Soc., Perkin Trans. 2*, 1996, 1325–1329.
39 C. M. Lagier, A. C. Olivieri and R. K. Harris, *J. Chem. Soc., Perkin Trans. 2*, 1998, 1791–1796.
40 D. C. Apperley, P. A. Chaloner, L. A. Crowe, R. K. Harris, R. M. Harrison, P. B. Hitchcock and C. M. Lagier, *Phys. Chem. Chem. Phys.*, 2000, **2**, 3511–3518.
41 T. Krachko, V. Lyaskovskyy, M. Lutz, K. Lammertsma and J. C. Slootweg, *Z. Anorg. Allg. Chem.*, 2017, **643**, 916–921.
42 J. S. Wenger and T. C. Johnstone, *Chem. Commun.*, 2021, **57**, 3484–3487.
43 J. S. Wenger, X. Wang and T. C. Johnstone, *Inorg. Chem.*, 2021, **60**, 16048–16052.
44 F. Kleemiss, O. V. Dolomanov, M. Bodensteiner, N. Peyerimhoff, L. Midgley, L. J. Bourhis, A. Genoni, L. A. Malaspina, D. Jayatilaka, J. L. Spencer, F. White, B. Grundkötter-Stock, S. Steinhauer, D. Lentz, H. Puschmann and S. Grabowsky, *Chem. Sci.*, 2021, **12**, 1675–1692.
45 L. K. Saunders, A. R. Pallipurath, M. J. Gutmann, H. Nowell, N. Zhang and D. R. Allan, *CrystEngComm*, 2021, **23**, 6180–6190.
46 D. G. Gilheany, *Chem. Rev.*, 1994, **94**, 1339–1374.
47 L. Zhao, S. Pan, N. Holzmann, P. Schwerdtfeger and G. Frenking, *Chem. Rev.*, 2019, **119**, 8781–8845.
48 R. F. W. Bader, *Chem. Rev.*, 1991, **91**, 893–928.

49 J. A. Dobado, H. Martínez-García, J. M. Molina and M. R. Sundberg, *J. Am. Chem. Soc.*, 1998, **120**, 8461–8471.
50 D. B. Chesnut and A. Savin, *J. Am. Chem. Soc.*, 1999, **121**, 2335–2336.
51 D. B. Chesnut, *J. Phys. Chem. A*, 2003, **107**, 4307–4313.
52 T. Yang, D. M. Andrada and G. Frenking, *Phys. Chem. Chem. Phys.*, 2018, **20**, 11856–11866.
53 J. S. Wenger, M. Weng, G. N. George and T. C. Johnstone, *Nat. Chem.*, 2023, **15**, 633–640.
54 B. Pan and F. P. Gabbaï, *J. Am. Chem. Soc.*, 2014, **136**, 9564–9567.
55 B. Lindquist-Kleissler, J. S. Wenger and T. C. Johnstone, *Inorg. Chem.*, 2021, **60**, 1846–1856.
56 F. Eckert, I. Leito, I. Kaljurand, A. Kütt, A. Klamt and M. Diedenhofen, *J. Comput. Chem.*, 2009, **30**, 799–810.
57 S. Tshepelevitsh, A. Kütt, M. Lõkov, I. Kaljurand, J. Saame, A. Heering, P. G. Plieger, R. Vianello and I. Leito, *Eur. J. Org. Chem.*, 2019, 6735–6748.
58 A. H. Latham and M. E. Williams, *Langmuir*, 2006, **22**, 4319–4326.
59 W. Biesta, B. van Lagen, V. S. Gevaert, A. T. M. Marcelis, J. M. J. Paulusse, M. W. F. Nielen and H. Zuilhof, *Chem. Mater.*, 2012, **24**, 4311–4318.